

# SYNTHESIS AND CHARACTERIZATION OF COORDINATION COMPLEXES DERIVED FROM A CARBAZOLE-BASED SCHIFF BASE LIGAND WITH TRANSITION METALS AND ZINC, AND EVALUATION OF THEIR BIOLOGICAL ACTIVITY

F.T. Saeed<sup>1\*</sup>, E.A. Sulliman<sup>2</sup>

<sup>1</sup>Department of Chemistry, College of science, University of Mosul, Iraq

<sup>2</sup> Department of Biochemistry, College of Medicine, University of Mosul, Iraq

\*e-mail: [farah-t-s@uomosul.edu.iq](mailto:farah-t-s@uomosul.edu.iq)

Received 11.03.2025

Accepted 16.07.2025

**Abstract:** A new Schiff base ligand obtained from carbazole was synthesized and structurally characterized. Its coordination complexes with Co (II), Ni (II), Cu (II), and Zn (II) ions were prepared for the first time and investigated through various spectroscopic techniques, including <sup>1</sup>H-NMR, UV-Vis, and FT-IR. Density Functional Theory (DFT) estimations were also employed to study the electronic structures, stability, and optimized geometries of the ligand and its complexes. The Co (II) and Ni (II) complexes exhibited an octahedral geometry with a general formula of [M(L)<sub>2</sub>Cl<sub>2</sub>], while Cu (II) and Zn (II) formed either square planar or tetrahedral geometries, depending on the coordination environment. Analysis of spectral and computational data suggested that nitrogen and oxygen atoms in the ligand actively participated in metal coordination. In antibacterial testing, the synthesized metal complexes demonstrated enhanced inhibition against *Klebsiella pneumoniae* and *Staphylococcus aureus* compared to the uncoordinated ligand, suggesting that complexation improved antimicrobial activity.

These findings highlight the novelty of the synthesized ligand–metal complexes and their potential in medicinal chemistry, particularly given their distinct structural and electronic characteristics.

**Keywords:** carbazole, transition metal complexes, DFT, biological activity, coordination chemistry

## Introduction

The versatility of Schiff base ligands in donor atom modification and ease of formation has made them central to research in both medicinal and catalytic coordination chemistry.

Among the many scaffolds used in Schiff base chemistry, carbazole and its derivatives have gained significant consideration due to their rich electronic structures and broad spectrum of pharmacological activities. The synthesis of carbazole-based compounds has been extensively explored using various synthetic methodologies, including palladium- and rhodium-catalyzed cross-coupling and C–H activation strategies, allowing the construction of diverse carbazole frameworks with functional modifications [1–3]. These methodologies have greatly expanded the utility of carbazole derivatives in materials science and medicinal chemistry [4, 5].

Carbazole-based compounds are known to indicate a wide range of biologic action, including anticonvulsant, antimicrobial, antimalarial, and anticancer effects. In addition to their pharmacological relevance, carbazole derivatives have demonstrated excellent optoelectronic properties and have been incorporated into organic light-emitting diodes (OLEDs), photoconductors, and photovoltaic apparatus [6–10]. This dual nature—biological and electronic—makes carbazole an appealing core structure for ligand design, particularly in coordination complexes.

Several studies have noted the synthesizing and classification of carbazole-containing metal complexes. Notably, Andrew and colleagues (2009) synthesized homoleptic transition metal complexes of the type (1,8-Ph<sub>2</sub>-3,6-Me<sub>2</sub>C<sub>12</sub>H<sub>4</sub>N)<sub>2</sub>M, where M = Cr, Mn, Fe, and Co. These complexes exhibited distinct coordination geometries and electronic characteristics [11]. X-ray crystallography data for selected complexes revealed characteristic N–M–N bond angles and the deflection of phenyl groups toward the metal centers. Moreover, magnetic susceptibility studies supported the high-spin nature of these bis-carbazole metal complexes, especially those involving Cr–Co ions, with theoretical calculations corroborating the experimental findings [12].

Despite these advances, reports on Schiff base ligands obtained from carbazole hydrazides and their transition metallic structure remain scarce. The present study addresses this gap by synthesizing a novel hydrazide ligand—ethyl 2-(9H-carbazol-9-yl)acetohydrazide—derived from carbazole. The major aim of this study is to synthesize and characterize a new Schiff base ligand derived from carbazole and to prepare and evaluate its novel coordination complexes with Co (II), Ni (II), Cu (II), and Zn (II). These metal complexes were classified using several spectroscopic and analytic techniques such as FT-IR, UV-Vis, and <sup>1</sup>H-NMR spectroscopy, elementary analysis, magnetic susceptibility, molar conductivity, and atomic absorption spectrometry. Their electronic structures and geometries were further explored using (DFT) calculations.

To the best of our knowledge, neither the synthesized ligand nor its coordination complexes with these metal ions have been previously reported. These complexes represent a recent class of carbazole-based Schiff base metal complexes, contributing novel insights into the coordination chemistry, electronic structure, and potential biological activity of carbazole-derived ligands.

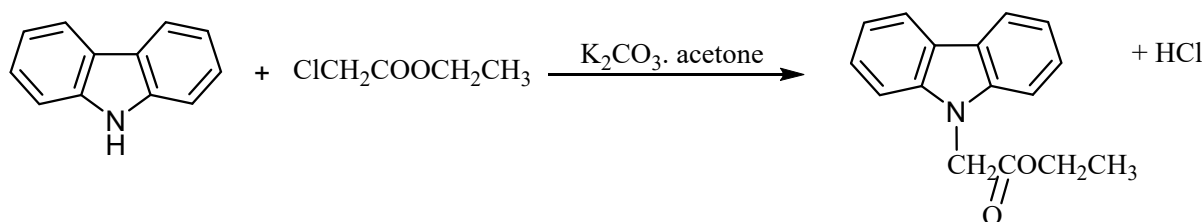
## Experimental Part

**Materials.** All compounds and solvents utilized in this investigation were of testing level and utilized without further purification. Carbazole, ethyl chloroacetate, anhydrous potassium carbonate, and hydrazine hydrate were purchased from Sigma-Aldrich. Metal(II) salts, including cobalt(II) chloride hexahydrate (CoCl<sub>2</sub>·6H<sub>2</sub>O), nickel(II) chloride hexahydrate (NiCl<sub>2</sub>·6H<sub>2</sub>O), copper(II) chloride dihydrate (CuCl<sub>2</sub>·2H<sub>2</sub>O), and zinc(II) chloride (ZnCl<sub>2</sub>), were also obtained from Sigma-Aldrich and used as received.

**Instrumentation and Characterization.** Elementary analyses for C, H, and N were using a Vario Micro Cube Elementary Analyzer. FT-IR spectra were recorded on a Shimadzu FTIR 8300 spectrophotometer using the KBr pellet method. UV-visible absorption spectra were measured with a PerkinElmer Lambda 2 spectrophotometer in dimethyl sulfoxide (DMSO). Proton nuclear magnetic resonance (<sup>1</sup>H NMR) spectra were recorded in DMSO-d<sub>6</sub> on a Bruker Avance DPX 250 MHz spectrometer using tetramethylsilane (TMS) as the internal reference. Magnetic sensitivity measurements were carried out at (25°C) using a Sherwood Scientific MK I Gouy balance. Metallic contents in the complexes were resolved by atomic absorption spectroscopy (Varian AA240 FS). Electrical conductivity measurements were performed in 1×10<sup>-3</sup> M dimethylformamide (DMF) solutions at room temperature using a Jenway 4070 conductivity meter.

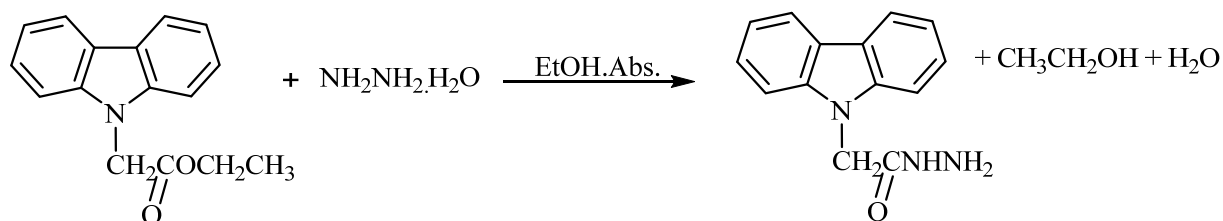
**Synthesizing of Ethyl 2-(9H-carbazol-9-yl)acetate (Compound A).** To synthesize compound A, carbazole (2.01 g, 0.012 mol) was dissolved in 25 mL of ethanol and combined with an equimolar amount of ethyl chloroacetate (1.47 g, 0.012 mol) in a reaction flask. Anhydrous potassium carbonate (0.013 g) was then added gradually under continuous stirring to facilitate the nucleophilic substitution. The reactive mixing was left to stir at ambient temperature for approximately 18 hours to ensure complete conversion.

Upon completion, the mixture was poured into 100 mL of ice-cold D.W., resulting in the precipitation of the crude product. The solid was composed by filtration, thoroughly cleansed with H<sub>2</sub>O to remove residual salts, and subsequently recrystallized from ethanol to afford pale brown crystals of the target ester intermediate, designated as compound A.



**Synthesizing of Ethyl 2-(9H-carbazol-9-yl)acetohydrazide (Ligand L).** By dissolving 2.50 grams of Compound A in 25 milliliters of ethanol. Then added 20 milliliters of hydrazine hydrate to

the mixture, incidentally stirring it for 5 hours followed by cooling it to external temperature. The solvent was then evaporated under decreasing pressure, and the resulting solid was gathered, dried, and purified through recrystallization in ethanol to yield the light hydrazide ligand L.



**Synthesis of Metal Complexes [M(L)Cl<sub>2</sub>] and [M(L)<sub>2</sub>Cl<sub>2</sub>] (M = Co(II), Ni(II), Cu(II), Zn(II)).** Solutions of ligand L (0.01 mol for 1:1 complexes or 0.02 mol for 2:1 complexes) in 25 mL ethanol were prepared. Separately, metal chloride salts (CoCl<sub>2</sub>·6H<sub>2</sub>O, NiCl<sub>2</sub>·6H<sub>2</sub>O, CuCl<sub>2</sub>·2H<sub>2</sub>O, or ZnCl<sub>2</sub>) (0.01 mole) were dissolved in 25 mL ethanol. The metal salt solutions were added dropwise to the refluxing ligand solutions under continuous stirring. Reflux was maintained for 3 hours. The resulting precipitates were filtered, cleaned up thoroughly with ethanol and diethyl ether, and dried under vacuum for 4 hr. to yield the corresponding metal complexes.

**Physical and Analytical Data.** The physical properties, melting/decomposition temperatures, yields, elemental analysis, and molar conductivity of the prepared compounds are summarized in Table 1.

**Table 1.** Physical Characteristics of the Produced Ligands and Metal Complexes

Seq.	Complexes	Coloring	m.p. (°C)	Yield %	Analysis (calc.)%					(Λ) cm <sup>2</sup> .ohm <sup>-1</sup> .mol <sup>-1</sup>
					C	H	N	M	Cl	
A	C <sub>16</sub> H <sub>15</sub> NO <sub>2</sub>	Pale brown	80–81	78	75.45 (75.87)	5.69 (5.97)	5.43 (5.53)	---	---	---
L	C <sub>14</sub> H <sub>13</sub> N <sub>3</sub> O	Pale yellow	248–250	81	70.15 (70.28)	5.40 (5.48)	17.29 (17.56)	----	---	---
1	[Co(L)Cl <sub>2</sub> ]	Blue	300 <sup>d</sup>	84	45.26 (45.68)	3.18 (3.29)	11.32 (11.42)	15.98 (16.01)	19.06 (19.26)	20
2	[Ni(L)Cl <sub>2</sub> ]	Brown	286 <sup>d</sup>	90	45.65 (45.71)	3.19 (3.29)	11.37 (11.42)	15.84 (15.96)	19.17 (19.27)	23
3	[Cu(L)Cl <sub>2</sub> ]	Dark brown	295 <sup>d</sup>	79	45.08 (45.12)	3.17 (3.25)	11.20 (11.27)	17.95 (16.05)	18.88 (19.02)	19
4	[Zn(L)Cl <sub>2</sub> ]	Light brown	279 <sup>d</sup>	88	44.78 (44.89)	3.13 (3.23)	11.18 (11.22)	17.38 (17.46)	18.83 (18.93)	16
5	[Co(L) <sub>2</sub> Cl <sub>2</sub> ]	Dark Blue	289 <sup>d</sup>	92	55.32 (55.46)	3.94 (3.99)	13.85 (13.86)	9.70 (9.72)	11.59 (11.69)	17
6	[Ni(L) <sub>2</sub> Cl <sub>2</sub> ]	Pale brown	280 <sup>d</sup>	85	55.43 (55.48)	3.92 (3.99)	13.84 (13.87)	9.61 (9.68)	11.68 (11.70)	22
7	[Cu(L) <sub>2</sub> Cl <sub>2</sub> ]	Brown	296 <sup>d</sup>	86	45.98 (45.78)	3.88 (3.97)	13.69 (13.62)	10.29 (10.33)	11.58 (11.06)	25
8	[Zn(L) <sub>2</sub> Cl <sub>2</sub> ]	White	267 <sup>d</sup>	93	54.79 (54.68)	3.84 (3.76)	13.68 (13.71)	10.52 (10.60)	11.48 (11.57)	27

d= decomposition temperature

## Results and Discussion

The synthesized hydrazide ligand (L), as depicted in Scheme 1, successfully coordinates with Co(II), Ni(II), Cu(II), and Zn(II) ions to yield a total of eight well-defined metal complexes. These were obtained in two stoichiometric ratios, 1 to 1 and 1 to 2 (metallic-to-ligand). All complexes demonstrated good solubilization in common organic solvents and exhibited thermal stability under dry conditions, with decomposition temperatures from 267°C to 300°C.

The physicochemical properties and elemental composition of the ligand and its corresponding complexes are abbreviated in Table 1. The experimental elemental analyses closely match the calculated values, confirming the proposed molecular formulas of the mono- and bis-ligand complexes:  $[M(L)Cl_2]$  and  $[M(L)_2Cl_2]$ , respectively.

Furthermore, molar conductivity performed in  $1 \times 10^{-3}$  M DMF solutions points out that all complexes behave as non-electrolytes, irrespective of the ligand-to-metallic ratio. The structural representations of these complexes are provided in Fig. 1, reflecting the expected geometrical configurations based on coordination chemistry principles.

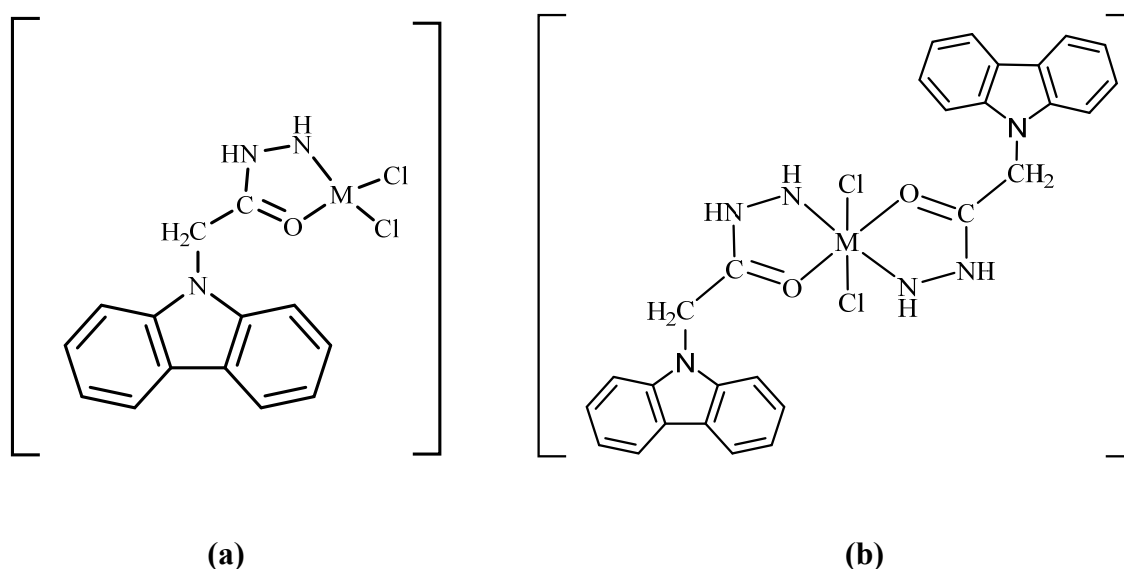


**Fig. 1.** The proposed structural formulas of compounds: (a)  $[M(L)Cl_2]$  and (b)  $[M(L)_2Cl_2]$

**Spectra of  $^1H$ -NMR:** The  $^1H$ -NMR spectral information for ligand L (Table 2) provides significant information about its structure and functional groups. A signal at 4.82 ppm corresponds to the methylene group ( $CH_2CO$ ) in the ligand backbone. The apex at 11.253 ppm is attributable to the amide proton (NH), and the peak at 8.121 ppm indicates the presence of an amine group ( $NH_2$ ).

The aromatic protons emerge as multiplets in the area from 7.136 to 8.122 ppm, corresponding to eight hydrogen atoms on the aromatic ring system. The chemical shifts and integrals are consistent with the expected texture of ligand L and confirm the successful synthesis.

The ligand's potential to act as a tridentate donor in metal complexation is supported by the presence of both amide (NH) and amine ( $NH_2$ ) groups, along with the aromatic ring system. These groups can coordinate with metal ions through nitrogen and oxygen atoms. Further confirmation of coordination sites was obtained through IR and UV-Vis spectral analysis.

**Table 2.**  $^1H$ -NMR Spectral Information of Ligand L in DMSO- $d_6$

Ligand	$\delta$ (ppm)	Assignment
A	1.284	$CH_2$ (s, 3H)
	4.14	$CH_2-CO$ (s, 2H)
	4.45	$CO-CH_2$ (s, 2H)

	7.138–8.122	Aromatic system (m, 8H)
L	4.82	CH <sub>2</sub> –CO (s, 2H)
	11.253	NH (s, 1H)
	8.121	NH <sub>2</sub> (s, 2H)
	7.136–8.121	Aromatic system (m, 8H)

Notes: *s* = singlet, *m* = multiplet

**IR- spectra.** The analysis of the IR spectral data presented in Table 3 provides evidence regarding the characteristics of ligand L and its metal complexes, helping to accurately identify the functional groups and their role in metal coordination.

The ligand L displays absorption peaks at 3417 cm<sup>-1</sup> and 3276 cm<sup>-1</sup> attributed to the stretch vibrating of  $\nu(\text{NHN})$ , confirming the existence of hydrazone groups in it. The pronounced peak, at 1735 cm<sup>-1</sup>, signifies the stretch of vibration of  $\nu(\text{C}=\text{O})$ , indicating the presence of a carbonyl group. The aromatic C–H stretching vibrations are noted at 3088 cm<sup>-1</sup>, while the aliphatic C–H stretch vibrations are noted at 2980 cm<sup>-1</sup>.

After mixing substances in a process called complexation, changes occur in the infrared bands detected; the alterations in the vibrations of C=O bonds stretching outwards are especially noticeable. The bands found between 1589 and 1665 cm<sup>-1</sup> in the metal mixtures either move to lower frequencies compared to when the ligands are free; this suggests that the oxygen atom in carbonyls is playing a role alongside the metal ions during coordination actions. In addition to this observation, the disappearance or weakening of  $\nu(\text{NHNH}_2)$  bands within the spectra serves as evidence confirming the involvement of nitrogen atoms within this coordination process.

Absorptions starting to show up in the 425–487 cm<sup>-1</sup> and 507–587 cm<sup>-1</sup> range suggest that there are stretching modes for metal-nitrogen and metal-oxygen connections taking place, which indicate some form of interaction between the ligand and the metal present. These bands confirm the formation of metal-nitrogen and metal-oxygen bonds and confirm the coordination of the ligand through the donor N and O atoms.

The spectrophotometer's limitations prevent the detection of an M–Cl band, which implies that Cl ions are bound to the metal center, as described in the suggested electrolytic nature of the complexes.

The changes in the IR spectrum suggest that the ligand functions as a chelating agent in two ways, either by binding through the oxygen or the hydrazone nitrogen atoms to create stable Metal chelates with octahedral structures in 1:2 (metal to ligand ratio) and tetrahedral or square planar shapes, in 1:1 complex.

The outcomes presented, along with the study and conductivity information, provide backing for the suggested coordination styles and the development of metal-ligand chelates. Every synthesized chemical was subjected to an IR spectral analysis. By using infrared spectra, one can determine the type of ligand-metal bond. While the bands obtained for  $\nu$  (C–H stretching of aliphatic group) at (2980, 2985 cm<sup>-1</sup>), (1742 cm<sup>-1</sup>) for (C=O stretching), and (1145 cm<sup>-1</sup>) for (C–O–C stretching) respectively support the creation of  $\nu$  (C–H stretching of aromatic ring) in the compound (A)'s IR spectra, the band at (3086 cm<sup>-1</sup>) supports this formation [14].

The formation of  $\nu(\text{C–H stretching of aromatic ring})$  is supported by the band at (3088) cm<sup>-1</sup> in the IR spectra of L [15].  $\nu(\text{NHNH}_2 \text{ stretching})$  bands were obtained at 3417 and 3276 cm<sup>-1</sup>, whereas the band (1735 cm<sup>-1</sup>) returned to the (C=O stretching). New bands featured in the variety of 507–587 cm<sup>-1</sup> and 425–478 cm<sup>-1</sup>, corresponding to the stretching vibrations of M–O and M–N bonds, respectively. These shifts—compared to the free ligand spectrum—confirm the coordination of the ligand to the metal ions and indicate that bond formation led to slight upfield or downfield frequency changes depending on the complex structure [16, 17]. Which points out the participation of nitrogen and oxygen atoms of the carbazole derivative in bonding [18, 19]. The M–Cl band is not detected because it falls below the limit of the spectrophotometer range, as indicated in this discussion regarding L coordinating with metal ions. In a tetradentate and octahedral manner, O M N is arranged [20]. The outcomes are detailed in the following Table 3.

**Table 3.** Characteristic IR Absorber Bands ( $\text{cm}^{-1}$ ) of the Ligand Ethyl 2-(9H-carbazol-9-yl)acetohydrazide (L) and Its Corresponding Metal Complexes

No.	Compound	$\nu(\text{C-H})$ Aliphatic	$\nu(\text{C-H})$ Aromatic	$\nu(\text{C=O})$	$\nu(\text{C-O-C})$	$\nu(\text{NHNH}_2)$	$\nu(\text{NH})$	$\nu(\text{M-N})$	$\nu(\text{M-O})$
A	$\text{C}_{16}\text{H}_{15}\text{NO}_2$	2985	3086	1742	1145	–	–	–	–
L	$\text{C}_{14}\text{H}_{13}\text{N}_3\text{O}$	2980	3088	1735	–	3417, 3276	–	–	–
1	$[\text{Co}(\text{L})\text{Cl}_2]$	2978	3045	1589	–	3417	3420	456	564
2	$[\text{Ni}(\text{L})\text{Cl}_2]$	2987	3046	1631	–	3417	3421	437	507
3	$[\text{Cu}(\text{L})\text{Cl}_2]$	2983	3045	1665	–	3417	3467	476	575
4	$[\text{Zn}(\text{L})\text{Cl}_2]$	2985	3046	1635	–	3417	3472	425	537
5	$[\text{Co}(\text{L})_2\text{Cl}_2]$	2986	3044	1643	–	3417	3478	457	577
6	$[\text{Ni}(\text{L})_2\text{Cl}_2]$	2984	3047	1629	–	3417	3476	443	547
7	$[\text{Cu}(\text{L})_2\text{Cl}_2]$	2985	3046	1631	–	3417	3469	427	587
8	$[\text{Zn}(\text{L})_2\text{Cl}_2]$	2984	3045	1626	–	3417	3456	487	557

**Magnetic Measurement and UV-Visible Spectra.** At ordinary room temperature, the magnetic moment values of the complexes 1, 2, and 3 were measured to be 4.4, 2.9, and 2.2 Bohr Magnetons (B.M.), respectively. These values are consistent with the expected ranges for tetrahedral geometries in Co(II), Ni(II), and Cu(II) complexes [21–23].

These reported values align with the expected range for spin tetrahedral shapes of Cobalt (II), Nickel (II), and Copper (II) based complexes [21–23].

In contrast, the magnetic moment values for complexes 5, 6, and 7 were recorded as 4.9, 2.8, and 1.76 B.M., respectively, which support the presence of octahedral geometries around the metal centers [24].

**UV-Visible light Spectroscopy.** The UV Visible light spectra of the ligand and its compounds show expected transitions. Absorption peaks are observed at  $36789 \text{ cm}^{-1}$  for  $\pi \rightarrow \pi^*$  transitions and at  $40324 \text{ cm}^{-1}$  for  $n \rightarrow \pi^*$  transitions., which are attributed to intra-ligand  $\pi \rightarrow \pi^*$  and  $n \rightarrow \pi^*$  transitions, respectively. In the spectra of the metal compounds, these transitions are slightly shifted, indicating coordination of the ligand to metal ions. Additional bands appearing in the range  $28797\text{--}37432 \text{ cm}^{-1}$  are attributable to ligand-to-metallic charge transfer (LMCT) transitions [25].

- Co (II) Complex (1): Exhibiting a broad band at  $14879 \text{ cm}^{-1}$ , assigned to the  ${}^4\text{A}_2(\text{F}) \rightarrow {}^4\text{T}_1(\text{P})$  transition, consistent with a tetrahedral geometry [26].
- Co (II) Complex (5): Shows bands at  $10186$ ,  $16168$ , and  $19560 \text{ cm}^{-1}$ , appointed to  ${}^4\text{T}_1\text{g}(\text{F}) \rightarrow {}^4\text{T}_2\text{g}(\text{F})$ ,  ${}^4\text{T}_1\text{g}(\text{F}) \rightarrow {}^4\text{A}_2\text{g}(\text{F})$ , and  ${}^4\text{T}_1\text{g}(\text{F}) \rightarrow {}^4\text{T}_1\text{g}(\text{P})$  transitions, point out an octahedral geometry [27].
- Ni (II) Complex (2): Displays a band at  $14653 \text{ cm}^{-1}$ , attributed to the  ${}^3\text{T}_1(\text{F}) \rightarrow {}^3\text{T}_1(\text{P})$  transition, suggesting a tetrahedral geometry [28].
- Ni (II) Complex (6): Shows three bands at  $10298$ ,  $15589$ , and  $23857 \text{ cm}^{-1}$  corresponding to  ${}^3\text{A}_2\text{g}(\text{F}) \rightarrow {}^3\text{T}_2\text{g}(\text{F})$ ,  ${}^3\text{A}_2\text{g}(\text{F}) \rightarrow {}^3\text{T}_1\text{g}(\text{F})$ , and  ${}^3\text{A}_2\text{g}(\text{F}) \rightarrow {}^3\text{T}_1\text{g}(\text{P})$  transitions, confirming an octahedral geometry [29].
- Cu (II) Complex (3): A broad band at  $14749 \text{ cm}^{-1}$  is assigned to  ${}^2\text{T}_2 \rightarrow {}^2\text{E}$  transitions, characteristic of a tetrahedral environment [30].
- Cu (II) Complex (7): Displays a band at  $15657 \text{ cm}^{-1}$  assigned to  ${}^2\text{B}_1\text{g} \rightarrow {}^2\text{A}_1\text{g}$  transition, suggesting an octahedral geometry [31,32].
- Zn (II) Complexes (4 and 8): Only show charge transfer bands at  $35876$  and  $35492 \text{ cm}^{-1}$ , respectively. This indicates a tetrahedral geometry for complex (4) and an octahedral geometry for complex (8) [33].

**Table 4.** Data of Electronic Spectral and Magnetic Moments of Ligand L and Its Metallic Complexes

No.	Complex	Bands (cm <sup>-1</sup> )	Suggested Transitions	Geometry	$\mu_{\text{eff}}$ (B.M.)
L	C <sub>14</sub> H <sub>13</sub> N <sub>3</sub> O	36789, 40324	$\pi \rightarrow \pi^*$ , $n \rightarrow \pi^*$	—	—
1	[Co(L)Cl <sub>2</sub> ]	42870, 41600, 32791, 14879	$\pi \rightarrow \pi^*$ , $n \rightarrow \pi^*$ , CT, <sup>4</sup> A <sub>2</sub> (F) → <sup>4</sup> T <sub>1</sub> (P)	Td	4.4
2	[Ni(L)Cl <sub>2</sub> ]	42623, 45110, 32916, 14653	$\pi \rightarrow \pi^*$ , $n \rightarrow \pi^*$ , CT, <sup>3</sup> T <sub>1</sub> (F) → <sup>3</sup> T <sub>1</sub> (P)	Td	2.9
3	[Cu(L)Cl <sub>2</sub> ]	43670, 38621, 29432, 14749	$\pi \rightarrow \pi^*$ , $n \rightarrow \pi^*$ , CT, <sup>2</sup> T <sub>2</sub> → <sup>2</sup> E	Td	2.2
4	[Zn(L)Cl <sub>2</sub> ]	45941, 42209, 35876	$\pi \rightarrow \pi^*$ , $n \rightarrow \pi^*$ , CT	Td	0.0
5	[Co(L) <sub>2</sub> Cl <sub>2</sub> ]	45151, 41575, 36901, 10186, 16168, 19560	$\pi \rightarrow \pi^*$ , $n \rightarrow \pi^*$ , CT, d-d transitions	Oh	4.9
6	[Ni(L) <sub>2</sub> Cl <sub>2</sub> ]	45161, 44790, 36955, 10298, 15589, 23857	$\pi \rightarrow \pi^*$ , $n \rightarrow \pi^*$ , CT, d-d transitions	Oh	2.8
7	[Cu(L) <sub>2</sub> Cl <sub>2</sub> ]	45727, 36250, 33582, 15657	$\pi \rightarrow \pi^*$ , $n \rightarrow \pi^*$ , CT, <sup>2</sup> B <sub>1g</sub> → <sup>2</sup> A <sub>1g</sub>	Oh	1.76
8	[Zn(L) <sub>2</sub> Cl <sub>2</sub> ]	46102, 39134, 35492	$\pi \rightarrow \pi^*$ , $n \rightarrow \pi^*$ , CT	Oh	0.0

**Note:** CT = Charge Transfer, Td = Tetrahedral, Oh = Octahedral

**Conductivity measurement.** The molar conductivity measurements for all compounds varied between 16 and 27  $\Omega^{-1} \cdot \text{cm}^2 \cdot \text{mol}^{-1}$  in DMF at a conc. of  $10^{-3}$  M, under standard temperature conditions, suggesting that these compounds exhibit non-electrolyte characteristics when dissolved in the solution [34]. The conductivity data is provided in Table 1.

**Calculation of Density Functional Theory (DFT).** The quantum chemistry endpoint derived from the DFT/B3LYP method presented in Table 5 provides information about specific physical and electronic characteristics of ligand L and its complexes. These include the energy gap space among the HOMO and LUMO orbitals ( $\Delta E$ ), chemical potential ( $\mu$ ), absolute hardness ( $\eta$ ), global softness (S), and electrophilicity index ( $\omega$ ). Collectively, these parameters help assess the stability and reactivity of the molecules [35, 36].

The energy gap ( $\Delta E$ ) between the HOMO and LUMO levels returns the chemical stability of a molecule; a wider gap suggests greater stability and lower reactivity. According to the data, the free ligand L has a  $\Delta E$  value of 3.678 eV, indicating higher stability than most of its complexes. In contrast, the [Co(L)<sub>2</sub>Cl<sub>2</sub>] complex exhibits the smallest energy gap (0.233 eV), suggesting it is the least stable and the most chemically reactive [37].

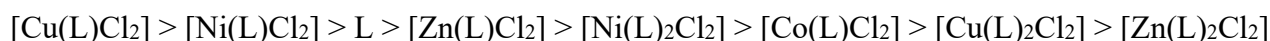
Molecular hardness ( $\eta$ ) is another stability indicator, where higher  $\eta$  values indicate more rigid and less reactive molecules. The free ligand L has a hardness of 1.839 eV, while [Cu(L)Cl<sub>2</sub>] and [Ni(L)Cl<sub>2</sub>] have values of 1.145 eV and 1.164 eV, respectively, indicating that they are comparatively stable.

The chemical potential ( $\mu$ ) describes the molecule's electron-accepting tendency. A more negative  $\mu$  indicates stronger electrophilic character and higher reactivity. For example, [Ni(L)Cl<sub>2</sub>] shows a chemical potential of -9.414 eV, suggesting high electrophilicity. However, [Cu(L)Cl<sub>2</sub>] has a positive  $\mu$  (+9.433 eV), which deviates from this trend.

Global softness (S), the inverse of hardness, also reflects reactivity. [Co(L)<sub>2</sub>Cl<sub>2</sub>], for instance, shows a high softness value (8.620 eV), indicating exceptional reactivity.

The electrophilicity index ( $\omega$ ), which reflects a molecule's ability to accept electrons, is highest for [Cu(L)Cl<sub>2</sub>] (38.856 eV) and [Ni(L)Cl<sub>2</sub>] (38.068 eV), indicating these are the most electrophilic and potentially reactive complexes.

Based on  $\Delta E$  and  $\omega$  values, the stability order of the studied compounds is:



This data shows that [Cu(L)Cl<sub>2</sub>] is the most stable and electrophilic compound, while [Zn(L)<sub>2</sub>Cl<sub>2</sub>] appears to be the least stable among those studied

The results provide an extensive insight into the chemical behavior and properties of the ligand and its metal complexes, suggesting potential applications in coordination chemistry and catalysis.

To evaluate molecular stability and responsiveness, the estimation of global rigidity ( $\eta$ ) and absolute softness ( $S$ ) is essential. Bond energy analysis indicates that the increase in bond energy of the complexes reflects a higher stability comparable to the free ligand.

Chemical properties, like chemical potential ( $\mu$ ), electrophilicity index ( $\omega$ ), global softness ( $S$ ), and hardness ( $\eta$ ), were determined for both the ligand and its complexes and are detailed in Table 5. All quantum chemical estimations were performed using the Gaussian 03 software, which is well-suited for modeling organic and coordination compounds. Molecular structures were visualized using GaussView 4.1.

Geometry optimizations were performed using the B3LYP functional and the 6-311G(d,p) basis set for C, N, O, and H atoms. According to the hard and soft acid–base (HSAB) principle, species with larger HOMO–LUMO energy gaps are considered harder (less reactive), which correlates with their stability. Pearson's definition of global hardness  $\eta$  can be expressed as:

$$\eta = \frac{1}{2}(\partial^2 E / \partial N^2)_{v(r)}$$

Where:

- $\mu = (\partial E / \partial N)_{v(r)}$
- $E$  = total energy
- $N$  = number of electrons under external potential  $v(r)$

Practically,  $\eta$  and  $\mu$  are estimated using ionization potential (IP) and electron affinity (EA):

$$\mu = -(\text{IP} + \text{EA})/2$$

$$\eta = (\text{IP} - \text{EA})/2$$

Koopmans' theorem provides a useful approximation that links molecular orbital energies to key reactivity descriptors. Specifically, the ionization potential (IP) and electron affinity (EA) are approximated as complying with:

$$\text{IP} \approx -E_{\text{HOMO}}, \text{EA} \approx -E_{\text{LUMO}}$$

Determined on this, the electronic chemical potential ( $\mu$ ) and chemical hardness ( $\eta$ ) can be defined as:

$$\mu = 2E_{\text{HOMO}} + E_{\text{LUMO}}, \eta = 2E_{\text{LUMO}} - E_{\text{HOMO}}$$

Alternatively, when using ionization potential and electron affinity directly:

$$\mu = -2\text{IP} + \text{EA}, \eta = 2\text{IP} - \text{EA}$$

These parameters are essential for understanding the stability and reactivity of molecular systems. The electrophilicity index ( $\omega$ ), introduced by Parr and co-workers, quantifies the electrophilic character of a molecule and is calculated using the following relation:

$$\omega = 2\eta\mu^2$$

In a conceptual DFT perspective, the potential of chemical substances  $\mu$  is described as the derivative of the electronic energy ( $E$ ) with regard to the number of electrons ( $N$ ) at a constant external potential  $v(r)$ :

$$\mu = (\partial N \partial E)_{v(r)}$$

Similarly, the absolute hardness  $\eta$  can be defined as:

$$\eta = \frac{1}{2}(\partial^2 N \partial \mu)_{v(r)}$$

Koopmans' approximation therefore supports the relationship between Pearson's concepts of absolute hardness/softness and the HOMO–LUMO energy gap, where IP and EA are directly correlated to the frontier orbital energies.

[ $E_{\text{LUMO}} - E_{\text{HOMO}}$ ] is the energy gap ( $\Delta E$ ) value. Table 5 shows the consequence of the calculations for each of these parameters for L and their composite. Understanding the characteristics and behavior of molecules, such as their kinetic stability, chemical reactivity, softness, and hardness, requires an analysis of the boundary molecular orbitals (HOMO) and LUMO. Since the compound's

stability has a minimum ( $\omega$ ) and a maximum (max), the prepared compounds' stability order is as follows. The HOMO and LUMO of L, the optimal structures, and the composite (Fig. 2) [41].

**Table 5.** The quantum characteristics of L and its compounds

No.	Complex	E LUMO	E HOMO	$\Delta E$	$\eta$	$\mu$	S	$\omega$
L	C <sub>14</sub> H <sub>13</sub> N <sub>3</sub> O	-3.046	-6.724	3.678	1.839	-4.885	0.543	6.488
1	[Co(L)Cl <sub>2</sub> ]	-0.596	-1.554	0.958	0.479	-1.075	2.087	1.206
2	[Ni(L)Cl <sub>2</sub> ]	-8.250	-10.578	2.328	1.164	-9.414	0.859	38.068
3	[Cu(L)Cl <sub>2</sub> ]	-8.288	-10.578	2.290	1.145	9.433	0.873	38.856
4	[Zn(L)Cl <sub>2</sub> ]	-0.591	-3.036	2.445	1.222	-1.813	0.818	1.344
5	[Co(L) <sub>2</sub> Cl <sub>2</sub> ]	-0.081	-0.314	0.233	0.116	-0.197	8.620	0.163
6	[Ni(L) <sub>2</sub> Cl <sub>2</sub> ]	-0.570	-1.072	0.502	0.251	-0.821	3.984	1.342
7	[Cu(L) <sub>2</sub> Cl <sub>2</sub> ]	-0.421	-0.793	0.372	0.186	-0.607	5.376	0.989
8	[Zn(L) <sub>2</sub> Cl <sub>2</sub> ]	-0.293	-0.571	0.278	0.139	-0.432	7.194	0.669

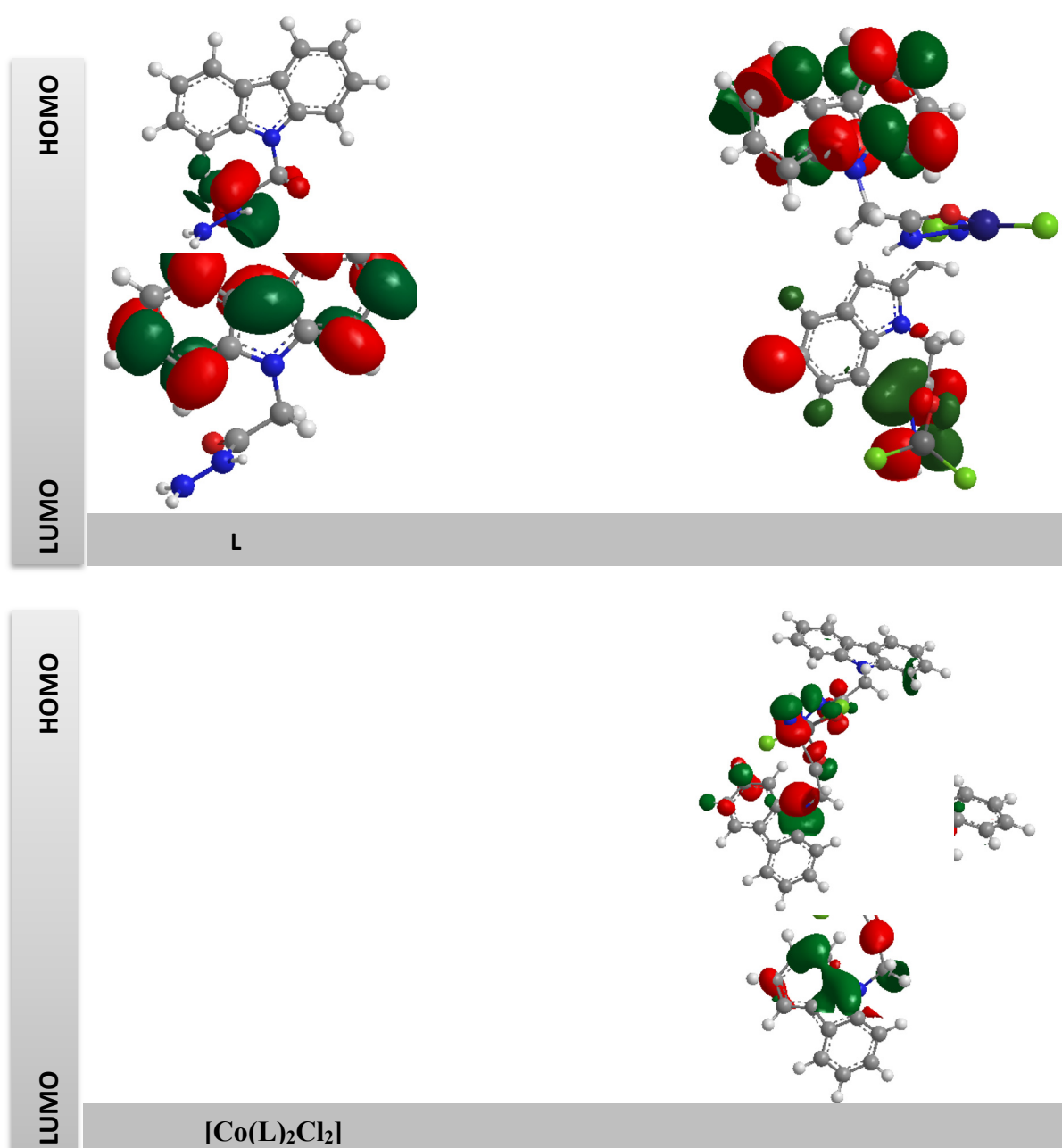


**Fig. 2.** The optimized structures and the HOMO and LUMO of the Ligand and complexes

**Antibacterial Activity.** The anti-microbial feature of free ligand (L) and its metallic structure were investigated against *Klebsiella pneumoniae* and *Staphylococcus aureus*. The outcome, summarized in Table 6 and Figure 3, indicates that metal complexation generally enhances antibacterial activity compared to the free ligand.

For *Klebsiella pneumoniae*, the ligand (L) exhibited an inhibition zone of 20 mm, while its metal complexes demonstrated improved activity: [Cu(L)Cl<sub>2</sub>] (26 mm), [Zn(L)Cl<sub>2</sub>] (25 mm), and [Co(L)Cl<sub>2</sub>] and [Ni(L)Cl<sub>2</sub>] (25 mm each). Though the increase in activity appears significant, the difference between the complexes and the ligand ( $\Delta = 5-6$  mm) must be interpreted in light of experimental error. Therefore, measurement uncertainty ( $\pm 1$  mm or more, depending on the diffusion method) should be reported to assess statistical significance.

Chelation is thought to enhance the antimicrobial behavior of metal complexes by promoting better membrane permeability and interaction with bacterial systems, which increases the lipophilicity of the ligand and enhances its ability to permeate bacterial membranes, interfering with enzymatic or metabolic processes. However, it is important to note that chelation theory alone cannot definitively explain antibacterial efficiency, and further biochemical studies are needed to validate these claims.

Against *Staphylococcus aureus*, the ligand showed weaker activity (12 mm), while the complexes [Zn(L)Cl<sub>2</sub>] and [Co(L)<sub>2</sub>Cl<sub>2</sub>] displayed stronger suppression zones of 18 mm and 19 mm. The order of antibacterial activity against *Klebsiella pneumoniae* was:

[Cu(L)Cl<sub>2</sub>] > [Zn(L)Cl<sub>2</sub>]  $\approx$  [Co(L)Cl<sub>2</sub>]  $\approx$  [Ni(L)Cl<sub>2</sub>] > [Ni(L)<sub>2</sub>Cl<sub>2</sub>] > [Cu(L)<sub>2</sub>Cl<sub>2</sub>] > [Co(L)<sub>2</sub>Cl<sub>2</sub>]  $\approx$  L

And against *Staphylococcus aureus*:

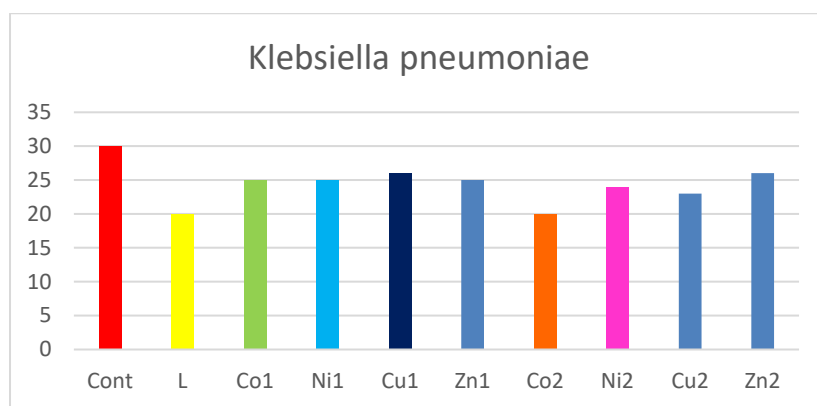
[Co(L)<sub>2</sub>Cl<sub>2</sub>] > [Zn(L)Cl<sub>2</sub>] > [Ni(L)<sub>2</sub>Cl<sub>2</sub>] > [Co(L)Cl<sub>2</sub>] > [Cu(L)Cl<sub>2</sub>] > [Cu(L)<sub>2</sub>Cl<sub>2</sub>] > [Ni(L)Cl<sub>2</sub>] > L

Ciprofloxacin, used as a standard, produced larger inhibition zones (30 mm for *K. pneumoniae* and 20 mm for *S. aureus*), outperforming all ligand and complex samples. Therefore, the statement that the tested compounds were "more effective than Ciprofloxacin" is not supported by the data and has been corrected.

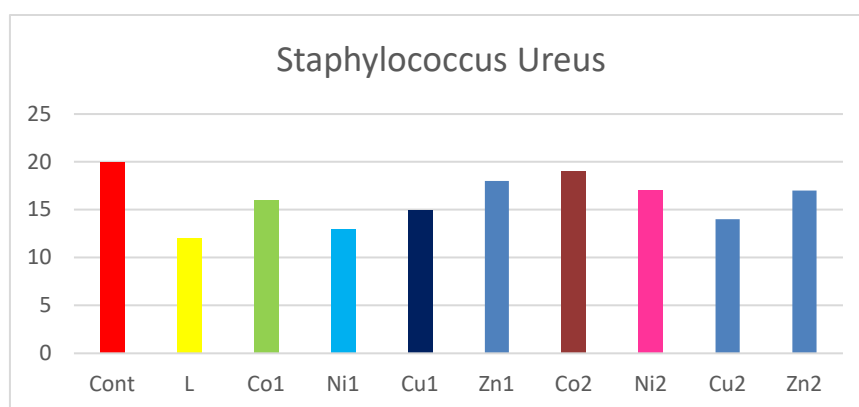
These findings suggest that complexation with metal ions enhances antibacterial potential, likely due to changes in lipophilicity, stability, and the ability to interfere with bacterial cell components. However, further testing, including MIC determination and statistical validation, is needed to fully confirm their efficacy and potential as antimicrobial agents against resistant bacterial strains.

**Table 6.** Anti-microbial activity of the Ligands and their compound

No.	sign	complex	<i>Klebsiella pneumoniae</i> (mm)	<i>Staphylococcus Aureus</i> (mm)
	L	C <sub>14</sub> H <sub>13</sub> N <sub>3</sub> O	20	12
1	Co1	[Co(L)Cl <sub>2</sub> ]	25	16
2	Ni1	[Ni(L)Cl <sub>2</sub> ]	25	13
3	Cu1	[Cu(L)Cl <sub>2</sub> ]	26	15
4	Zn1	[Zn(L)Cl <sub>2</sub> ]	25	18
5	Co2	[Co(L) <sub>2</sub> Cl <sub>2</sub> ]	20	19
6	Ni2	[Ni(L) <sub>2</sub> Cl <sub>2</sub> ]	24	17
7	Cu2	[Cu(L) <sub>2</sub> Cl <sub>2</sub> ]	23	14
8	Zn2	[Zn(L) <sub>2</sub> Cl <sub>2</sub> ]	26	17
	Control		30	20



(a) *Klebsiella pneumoniae*



(b) *Staphylococcus aureus*

**Fig. 3.** The antibacterial properties of substances against (a) *Klebsiella pneumonia* bacteria and (b) *Staphylococcus aureus*

## Conclusion

This research examines the creation and analysis of transition metal compounds using Schiff base ligands that function as bidentate in Type (I) complexes and tetradentate in Type (II) complexes when combined with metal in molar ratios of 1:1 and 2:1, respectively. The properties of the ligand and the general compositions of the resulting compounds were identified through a range of physical and spectroscopic techniques.

To gain an understanding of the molecular properties of the created compound, Density Functional Theory estimations were performed to reveal details about the best geometries and electronic stability of structures. The phrase "best geometries" is employed instead of "ideal shape" to accurately convey the scientific concept.

After testing the compound on two types of bacteria, it was found that the metallic compound had a greater antibacterial impact than the free ligand alone, indicating that these metal-based compounds could be promising candidates for future antimicrobial medications.

## References

1. Marappan P.K., Mahantesh G., Amaladass P., Chitrasu M., Vasudevan D. Recent synthetic strategies for the construction of functionalized carbazoles and their heterocyclic motifs enabled by Lewis acids. *RSC Advances*, 2023, Vol. 46(13), p. 32596-32626. DOI: [10.1039/d3ra06396h](https://doi.org/10.1039/d3ra06396h)
2. Xu W., Wang G., Xie X., Liu Y. Gold(I)-Catalyzed Formal Intramolecular Dehydro-Diels–Alder Reaction of Ynamide-ynes: Synthesis of Functionalized Benzo[b] carbazoles, *Organic Letter*, 2018, Vol. 20(11), p. 3273-3277. DOI: [10.1021/acs.orglett.8b01145](https://doi.org/10.1021/acs.orglett.8b01145)

3. Raju P., Mohanakrishnan A.K. Synthetic Approach to Dictyodendrins: A Facile Synthesis of Pyrrolo[2,3-c]carbazole, Pyrrolodibenzothiophene, and Benzo[e]indole. *Eur. J. Org Chem.*, 2016, **Vol. 2016(25)**, p. 4361–4371. DOI: [10.1002/ejoc.201600674](https://doi.org/10.1002/ejoc.201600674)
4. Munawar S., Zahoor A.F., Mansha A., Bokhari T.H., Irfan A. Update on novel synthetic approaches towards the construction of carbazole nuclei: a review. *RSC Advances*, 2024, **Vol. 14**, p. 2929-2946. DOI: [10.1039/D3RA07270C](https://doi.org/10.1039/D3RA07270C)
5. Çapan İ., Hawash M., Jaradat N., Sert Y., Servi R., Koca İ. Design, synthesis, molecular docking and biological evaluation of new carbazole derivatives as anticancer, and antioxidant agents. *BMC Chem.*, 2023, **Vol. 17**, 60. DOI: [10.1186/s13065-023-00961-y](https://doi.org/10.1186/s13065-023-00961-y)
6. Srivastava S.K., Srivastava S., Srivastava S.D. Synthesis of new carbazolyl-thiadiazol-2-oxo-azetidines Antimicrobial, anticonvulsant and anti-inflammatory agents. *Indian J. Chem.*, 1999, **Vol. 38B(02)**, p. 183-187.
7. Hagiwara H., Choshi T., Fujimoto H., Sugino E., Hibino, S.A. Novel total synthesis of antibiotic carbazole alkaloid carbazomycin G. *Tetrahedron*, 2000, **Vol. 56(32)**, p. 5807–5811. DOI: [10.1016/S0040-4020\(00\)00543-3](https://doi.org/10.1016/S0040-4020(00)00543-3)
8. Bhat M.A., Al-Omar M., Khan A.A., Alanazi A., Naglah A. Synthesis and antihepatotoxic activity of dihydropyrimidinone derivatives linked with 1,4-benzodioxane. *Drug Design, Development and Therapy*, 2019, **Vol. 13**, p. 2393–2404. DOI: [10.2147/DDDT.S198865](https://doi.org/10.2147/DDDT.S198865)
9. Nagaraj A., Sanjeeva Reddy C. Synthesis and biological study of novel bis-chalcones, bis-thiazines and bis-pyrimidines, *J. Iran. Chem. Soc.*, 2008, **Vol. 5**, p. 262-267. DOI: [10.1007/BF03246116](https://doi.org/10.1007/BF03246116)
10. El-Emarya T.I., Abd El-Aala H.A.K., Mohamed Sh.K. New Trend in Carbazole Based Structure: Part 1: Synthesis and Characterization of Assorted Heterocycles Based 3-(9H-carbazol-9-yl)propane hydrazide as Potential Bioactive Compounds. *Int. J. Pharm. Sci. Rev. Res.*, 2018, **Vol. 53(2)**, p. 7-14.
11. Morin J.F., Leclerc M., Ades D., Siove A. Polycarbazoles: 25 Years of Progress. *Macromol. Rapid Commun.*, 2005, **Vol. 26(10)**, p. 761-778. DOI: [10.1002/marc.200500096](https://doi.org/10.1002/marc.200500096)
12. Kim D., Lee J.K., Kang S.O., Ko J. Molecular engineering of organic dyes containing N-aryl carbazole moiety for solar cell. *Tetrahedron*, 2007, **Vol. 63(9)**, p. 1913-1922. DOI: [10.1016/j.tet.2006.12.082](https://doi.org/10.1016/j.tet.2006.12.082)
13. Ashley A.E., Cowley A.R., Green J.C., Johnston D.R., Watkin D.J., Kays D.L. Synthesis and Characterisation of Low-Coordinate Transition-Metal Complexes Stabilised by Sterically Demanding Carbazolido Ligands. *European Journal of Inorganic Chemistry*, 2009, **Vol. 17**, p. 2547-2552. DOI: [10.1002/ejic.200900170](https://doi.org/10.1002/ejic.200900170)
14. Zeyrek C.T., Elmali A., Elerman Y., Svoboda I. Crystal structure and magnetic exchange interaction in a binuclear copper (II) schiff base complex with a bridging m-phenylenediamine ligand. *Zeitschrift für Naturforschung B*, 2005, **Vol. 60(2)**, p.143-148. DOI: [10.1515/znb-2005-0203](https://doi.org/10.1515/znb-2005-0203).
15. Saeed F.T., Jasim U.Z. Synthesis and Characterization of new Mn(II),Co(II),Ni(II),Cu(II),Zn(II) and Cd(II) complexes with [(z)-3((6-aminopyridine-2-yl) imino) indolin-2-one] ligand. *Chemical Problems*, 2024, **Vol. 22(1)**, p. 103-114. DOI: [10.32737/2221-8688-2024-1-103-114](https://doi.org/10.32737/2221-8688-2024-1-103-114)
16. Srivastava K.P., Kumar A., Singh R. Bivalent transition metal complexes of tridentate Schiff base ligands: an ecofriendly study. *J.Chem.Pharm. Res.* 2010, **Vol. 6 (2)**, p. 68-77.
17. Divya K., Gayathri B.H. Synthesis, Characterisation and Antimicrobial Study of Cobalt (II) Complex of A Schiff Base Derived from Isonicotinic Acid Hydrazide and 4-Chlorobenzaldehyde. *International Journal of Pharmaceutical Sciences Review and Research*, 2020, **Vol. 65(1)**, p. 83–87. DOI: [10.47583/ijpsrr.2020.v65i01.011](https://doi.org/10.47583/ijpsrr.2020.v65i01.011).
18. Keypour H., Salehzadeh S., Parish R.V. Synthesis of Two Potentially Heptadentate (N<sub>4</sub>O<sub>3</sub>) Schiff-base Ligands Derived from Condensation of Tris(3-aminopropyl)-amine and Salicylaldehyde or 4-Hydroxysalicylaldehyde. Nickel(II) and Copper(II) Complexes of the Former Ligand. *Molecules*, 2002, **Vol. 7(2)**, 140. DOI: [10.3390/70200140](https://doi.org/10.3390/70200140)

19. Pathan A.H., Naik G.N., Bakalae R.P., Machakanur S.S., Gudasi K.B. Ligation behavior of new mononucleating NOO ethyl pyruvate Schiff base towards 3d metal (II) ions: an emphasis on antiproliferative and photocleavage property. *Applied Organometallic Chemistry*. 2012, **Vol. 26(3)**, p. 148- 155. DOI: [10.1002/aoc.2831](https://doi.org/10.1002/aoc.2831)
20. Buttrus N.H., Hussian A.K., AL-Allaf T.A.K. Synthesis and characterization of new trinuclear Palladium (II) and Platinum (II) complexes containing phosphorus-sulphur Ligands. *Asian J. Chem.*, 2003, **Vol. 15(3)**, p. 1617-1622.
21. Nicholls D. *The Chemistry of Iron, Cobalt and Nickel*. Pergamon Press. Oxford. 1973, Edt. P. 1037. 1087. 1088. 1090. 1091. 1093. 1151. 1154.
22. Patel K.S., Ikekwere P.O. Magnetic and spectral properties of Cu (II) cyanobenzoates. *Journal of Inorganic and Nuclear Chemistry*, 1981, **Vol. 43(1)**, p. 51-55. DOI: [10.1016/0022-1902\(81\)80436-8](https://doi.org/10.1016/0022-1902(81)80436-8)
23. Kabanos T.A., Tsangaris J.M. Deprotonated And Non-Deprotonated Complexes Of N-(2-Aminophenyl) Pyridine-2- Carboxamide And N-(3-Aminophenyl) Pyridine-2-Carboxamide With Co (II), Ni (II), Cu (II) and Pd (II). *Journal of Coordination Chemistry*, 1984, **Vol. 13(2)**, p. 89-103. DOI: [10.1080/00958978408079760](https://doi.org/10.1080/00958978408079760)
24. Salih E.M., Saeed F.T. Synthesis and Characterization of Some Transition Metal Complexes with Bis(o-aminophenyl)Disulfide Alkane Ligands. *Egyptian Journal of Chemistry*, 2021, **Vol. 64(11)**, p. 6821 – 6826. DOI: [10.21608/EJCHEM.2021.78022.3815](https://doi.org/10.21608/EJCHEM.2021.78022.3815)
25. Shokohi-Pour Z., Chiniforoshan H., Momtazi-Borojeni A.A., Notash B. A novel Schiff base derived from the gabapentin drug and Cu(II) complexes synthesis, interaction with DNA/ protein and cytotoxic activity. *Polyhedron*, 2016, **Vol. 162**, p. 34-44. DOI: [10.1016/j.jphotobiol.2016.06.022](https://doi.org/10.1016/j.jphotobiol.2016.06.022)
26. Rakhi C., Shelly. Spectral and pharmacological study of Cu(II), Ni(II) and Co(II) coordination complexes. *Res.J. Chem. Sci.*, 2011, **Vol. 5(1)**, p. 87-90.
27. Chandra S., Tyagl M., Refat M.S. Spectroscopic, thermal and antibacterial studies on Mn(II) and Co(II) complexes derived from thiosemicarbazone. *J. Serb. Chem. Soc.* 2009, **Vol. 74(8-9)**, p. 907-915.
28. Saleem H.S., Mostafa M., Stefan S.L., Abdel-Aziz E. Structural diversity of 3d complexes of an isatinic quinolyl hydrazine. *Research Journal of Chemical Sciences*, 2011, **Vol. 1(5)**, p. 67-72.
29. Zalov A.Z., İsgenderova K.O., Askerova Z.G. Spectrophotometric research into interaction nickel (II) with 1-(2-pyridylazo)-2-hydroxy-4-mercaptofenol and aminophenols. *Chemical Problems*, 2021, **Vol. 19(3)**, p. 150-159. DOI: [10.32737/2221-8688-2021-3-150-159](https://doi.org/10.32737/2221-8688-2021-3-150-159)
30. Kulkarni P.A., Habib S.I., Saraf V.D., Deshpande M.M. Synthesis, spectral analysis and antimicrobial activity of some new transition metal complexes derived from 2,4-dihydroxy acetophenones. *Res. J. Pharm. Bio. Chemical Sci.*, 2012, **Vol. 3(1)**, p. 107-113.
31. Hassan S.S., Ibrahim S.K., Mahmoud M.A. Synthesis, characterization and theoretical study of some transition metal complexes with N-(4-(dimethyl amino benzylidene)benzo[d] thiozal-2-amine). *IOP Conference Series: Material Science and Engineering*. 2018, **Vol. 454**, 012124. DOI: [10.1088/1757-899X/454/1/012124](https://doi.org/10.1088/1757-899X/454/1/012124)
32. Bhattacharya R., Ray M.S., Dey R., Righi L., Bocelli G., Ghosh A. Synthesis, crystal structure and thermochromism of benzimidazolium tetrachlorocuprate: (C<sub>7</sub>H<sub>7</sub>N<sub>2</sub>)<sub>2</sub>[CuCl<sub>4</sub>]. *Polyhedron*. 2003, **Vol. 21(25-26)**, p. 2561-2565. DOI: [10.1016/S0277-5387\(02\)01237-8](https://doi.org/10.1016/S0277-5387(02)01237-8)
33. Nabeel B.H., Farah S.T. Synthesis and structural studies of some transition metal complexes of Bis-(benzimidazole-2-thio)ethane, propane and butane ligands. *Research Journal of Chemical Sciences*, 2012, **Vol. 2(6)**, p. 43-49.
34. Abdjbar R.R., Saeed F.T. Synthesis and characterization of Mn<sup>+2</sup>, Co<sup>+2</sup>, Ni<sup>+2</sup>, Cu<sup>+2</sup> and Zn<sup>+2</sup> complexes with 4-(2-(benzo-1,3-dioxol-5-yl)-4,5-diphenyl-2,5-dihydro-1H-imidazol-1-yl)aniline and evaluation of its biological activity. *Chemical Problems*, 2024, **Vol. 22(2)**, p.197-210. DOI: [10.32737/2221-8688-2024-2-197-210](https://doi.org/10.32737/2221-8688-2024-2-197-210)
35. Abu-Dief A.M., Alotaibi N.H., Al-Farraj E.S., Qasem H.A., Alzahrani S., Mahfouz M.K., Abdou A. Fabrication, structural elucidation, theoretical, TD-DFT, vibrational calculation and molecular

- docking studies of some novel adenine imine chelates for biomedical applications. *Journal of Molecular Liquids*, 2022, **Vol. 365**, 119961. DOI:[10.1016/j.molliq.2022.119961](https://doi.org/10.1016/j.molliq.2022.119961).
36. Mohamed G.G., Mahmoud W.H., Refaat A.M. Nano-Azo Ligand and Its Superhydrophobic Complexes: Synthesis, Characterization, DFT, Contact Angle, Molecular Docking, and Antimicrobial Studies. *Journal of Chemistry*, 2020, Article ID 6382037, 19 pages. DOI: [10.1155/2020/6382037](https://doi.org/10.1155/2020/6382037).
  37. Chattaraj P.K., Roy D.R. Update 1 of: electrophilicity index. *Chemical reviews*, 2007, **Vol. 107(9)**, p. PR46-PR74. DOI: [10.1021/cr078014b](https://doi.org/10.1021/cr078014b).
  38. Choudhury N. Importance of Theoretical and Computational Chemistry in State-of-the-art Chemistry Research. *R & D in Theoretical & Computational Chemistry*, 2024, p. 15-19
  39. Pearson R.G. Chemical hardness and density functional theory. *Journal of Chemical Sciences*, 2005, **Vol. 117**, p. 369-377.
  40. Tandon H., Chakraborty T., Suhag V. A fundamental approach to compute atomic electrophilicity index. *Journal of Mathematical Chemistry*, 2020, **Vol. 58**, p. 2188-2196. DOI: [10.1007/s10910-020-01176-5](https://doi.org/10.1007/s10910-020-01176-5)
  41. Tsuji Y., Yoshizawa K. From infection clusters to metal clusters: significance of the lowest occupied molecular orbital (LOMO). *ACS omega*, 2021, **Vol. 6(2)**, p. 1339-1351. DOI: [10.1021/acsomega.0c04913](https://doi.org/10.1021/acsomega.0c04913)
  42. Thangadurai T.D., Natarajan K. Mixed ligand complexes of ruthenium (II) Containing  $\alpha,\beta$ -Unsaturated  $\beta$ -ketoamines and their antibacterial activity. *Transition metal Chemistry*, 2001, **Vol. 26**, p. 500-504. DOI: [10.1023/A:1011099517420](https://doi.org/10.1023/A:1011099517420)